# A high pressure die cast magnesium alloy with superior thermal conductivity and high strength

Rong, Jian; Zhu, J.; Xiao, Wenlong; Zhao, Xinqing; Ma, Chaoli

**DOI**
10.1016/j.intermet.2021.107350

**Publication date**
2021

**Document Version**
Accepted author manuscript

**Published in**
Intermetallics

# A high pressure die cast magnesium alloy with superior thermal conductivity and high strength

Jian Rong[a], Jia-Ning Zhu[b], Wenlong Xiao[a,*], Xinqing Zhao[a], Chaoli Ma[a]

[a] Key Laboratory of Aerospace Advanced Materials and Performance of Ministry of Education, School of Materials Science and Engineering, Beihang University, Beijing 100191, China

[b] Faculty of Mechanical, Maritime, and Materials Engineering, Delft University of Technology, The Netherlands

## Abstract

Thermal conductivity is a key parameter for high performance material needed for electronic devices. While most commercially used Mg foundry alloys exhibit low thermal conductivities. In this work, we developed an Mg–3RE–0.5Zn alloy that is suitable for high pressure die cast (HPDC) ultrathin wall cellphone components. The thermal conductivity of this alloy was measured to be 133.9 W/(m·K) at room temperature, approximately 85% that of pure Mg (156 W/(m·K)). Meanwhile, it exhibited acceptable room-temperature mechanical properties with high yield strength of ~153 MPa, ultimate tensile strength of ~195 MPa, and elongation of ~4.3%. The excellent combination of superior thermal conductivity and high strength is attributed to low solute atoms in the α-Mg matrix and the formation of networked $(Mg, Zn)_{12}RE$ eutectic phase. The results from this study will be helpful for developing new HPDC Mg alloys with more excellent performances and promoting the wider application of Mg alloys.

***Keywords:*** Magnesium alloys; Microstructure; Thermal conductivity; Mechanical properties; High pressure die casting.

## 1. Introduction

Over the last decade, magnesium (Mg) alloys have been attracting increasing interest for applications in electric products, automobile, and aerospace industries because of their low density, high specific strength, and good electromagnetic shielding [1, 2]. Among them, the demand for high-thermal-conductivity Mg alloys with high mechanical performance is increasing rapidly in mobile communication devices, since high thermal conductivity ensures uniform temperature distribution

* Corresponding author: Tel: +86-10-8233 8631; Fax: 86-10-8233-8631;
E-mail: wlxiao@buaa.edu.cn (Wenlong Xiao).

which reduces thermally induced stresses and thus prolongs the service life of structural components [3, 4]. For high efficiency, most Mg alloys in mobile communication devices are high pressure die casting (HPDC) due to its inherent high rate of productivity and consequent relatively low cost for mass production [5, 6]. However, the most commercially used HPDC Mg–Al based alloys, such as Mg–9Al–1Zn-0.3Mn (wt.%, AZ91D), Mg–6Al–0.3Mn (wt.%, AM60) and Mg–2Al–1Si (wt.%, AS21), show poor room-temperature thermal conductivity owing to the solid solution of Al. For example, the thermal conductivity of AZ91D and AS21 alloy is 51.2 and 68 W/(m·K) at room temperature, respectively [7, 8]. Furthermore, an alloy used as a structural component must possess not only qualified heat dissipation capability but also sufficient strength, while the balance between the thermal conductivity and mechanical strength is a long-term challenge [9–11]. It is necessary to develop high–thermal–conductivity HPDC Mg alloys with good mechanical properties and acceptable castability for the widespread applications.

At present, the Mg alloys having thermal conductivities higher than 100 W/(m·K) are mainly based on Mg–Zn alloy system, such as Mg–3RE–3Zn (wt.%, EZ33A), Mg–5Zn–1Zr (wt.%, ZK51A) and Mg–6Zn–3Cu (wt.%, ZC63) foundry alloys [12], and the Mg–2Zn–Zr and Mg–5Zn–1Mn wrought alloys [13, 14]. However, these Mg-Zn based alloys are not suitable for high pressure die casting. The existing strategy of designing heat-dissipating Mg alloys is to reduce solute atoms in the α-Mg matrix and second phases at the expense of strength [9]. Many literatures have confirmed the influence of second phases on the thermal conductivity is much weaker than solute atoms [10, 15, 16]. Thus, it is possible to develop high-thermal-conductivity Mg alloys with high strength and acceptable castability by adding proper alloying elements. La and Ce elements seem to be potential elements for the above purpose due to their low solubility in the Mg matrix, showing a weak effect on the thermal conductivity of Mg alloys [17, 18]. Furthermore, they can refine grain structure and mainly exist in the form of $Mg_{12}RE$ intermetallic compounds, which contributes to enhancing the yield strength [10, 19, 20]. The HPDC Mg–La–Zn (HP2) with excellent creep resistance especially at elevated temperatures, has been successfully developed for powertrain application [21]. However, to our knowledge, the thermal properties of these HPDC Mg-RE-Zn alloys have been rarely studied.

In this work, a superior thermal conductivity and high strength of Mg–3RE–0.5Zn (EZ30) alloy (weight percentage, also for hereafter not mentioned) was designed for ultrathin walled electric components, where RE is Ce-rich mischmetal (65.24 Ce and 34.45 La) due to its low cost. Previous research confirmed that the addition of Zn could improve the die castability while having a weak influence on the thermal conductivity [9, 22]. The reason for the 0.5wt.% Zn addition is to improve the fluidity of alloy without losing thermal conductivity obviously. The microstructure, thermal properties, and mechanical properties of the HPDC EZ30 alloy were studied. The goal of this study was to develop an HPDC Mg alloy with a good combination of high thermal conductivity and high strength, which may be used as heat dissipation structural components of 5G smartphones.

## 2. Alloy design and Experimental Procedures

### 2.1 Thermo-Calc calculation

The commercial Thermo-Calc software and TTMG4 database were employed for designing alloying compositions. To investigate the content of Zn on the maximum solid solubility of RE and precipitation temperature of MgZn, isopleths along RE axis through Mg-RE (Ce+La)-Zn pseudo-ternary phase diagram were calculated. The solidification sequence was evaluated by using the Scheil model. The temperature increment was set to be 10 °C in all simulations.

### 2.2 Fabrication and characterizations

Commercial pure Mg (99.9%), pure Zn (99.9%), and Mg–30 wt.% RE master alloy were used as the raw materials. the alloy was melted in an electric resistance furnace under the protection of a gas mixture of $CO_2$ and $SF_6$. Before HPDC, the melt was refined, degassed, and held at ~720 °C. The actual composition of the Mg-3RE-0.5Zn alloy was measured to be Mg–2.45Ce–0.59La–0.48Zn–0.043Mn–0.013Si using inductively coupled plasma-atomic emission spectrometry (ICP–AES). HPDC was carried out on an IMPRESS 200T cold-chamber machine using a steel mold for producing Mg smartphone components with a minimum wall thickness of ~0.4mm. The parameters of the HPDC process used in this study were as follow: injection pressure, 60 MPa; ram velocity, 2.5 $m \cdot s^{-1}$; die holding time, ~5 s; mold temperature, ~260 °C. After HPDC, the real product with no hot cracking was achieved and presented in Fig. 1, indicating good die castability.

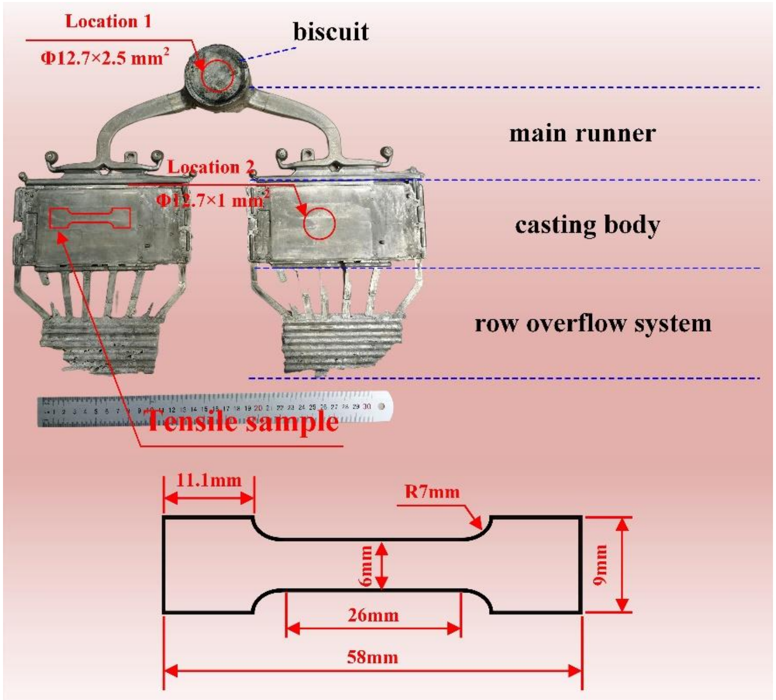


Fig. 1. The product image of the HPDC EZ30 alloy; inset: the size and location of testing samples for thermal conductivity and tension.

The size and location of testing samples for thermal conductivity are shown in Fig. 1. To avoid the influence of casting defects, the sample with rarely less defects was chosen for testing. The thermal diffusivity (α) for the biscuit (location 1) and the thin-wall casting body (location 2) was measured by the laser flash method at room temperature using a NETZSCH LFA 457 instrument. Room-temperature density ($\rho$) measurement was carried out by the Archimedes method. The heat capacity ($C_p$, Φ4.5 × 0.5mm) was determined using a NETZSCH DSC 204F1 Phoenix calorimeter. The testing of thermal diffusivity, density, and heat capacity was conducted at least 3 times for accuracy of the results. The thermal conductivity (λ) of the studied alloy was calculated by the following equation:

$$\lambda = \alpha \cdot \rho \cdot C_p$$

The tensile sample was cut from the location marked by the red line in Fig. 1 and the size of tensile samples was also presented in Fig. 1. The room-temperature tensile test was conducted on an Instron 8801 universal testing machine equipped with an extensometer at room temperature under a strain rate of $3.0\times10^{-3}$ $s^{-1}$. To keep good repeatability, six tensile samples were tested and average mechanical properties were recorded. Phase constituents were examined by X-ray diffraction (XRD, Rigaku RINT–2000, Japan) with Cu Kα radiation at the voltage of 40 kV at a scanning speed of 4 degrees/min. The microstructures were characterized by BX51 optical microscope (OM), JSM–7001F field emission scanning electron microscopy (FESEM) and JEM–2100F transmission electron microscopy (TEM) equipped with an INCA–X–Max energy dispersive spectrometer (EDS). The grain size distribution and average grain size were measured by Nano Measure software based on fifteen SEM-BSE images with low magnification. The solidification behavior was analyzed using the differential thermal analysis (DTA, SDT600, America) with cooling and/or heating rate of 10 K/min under the protection of Ar gas atmosphere.

## 3. Result and discussion

Pseudo–binary Mg–RE phase diagram (i.e. 0.0 wt.% Zn addition) was firstly calculated. As shown in Fig. 2 (a), the maximum solid solubility of RE in α-Mg is ~1.12 wt.%, and only α-Mg and $Mg_{12}RE$ will be formed after solidification within the RE content range from 0 to 5 wt.%. For avoiding the embrittlement induced by the large-size RE–containing intermetallic phase, the addition amount of RE was designed as 3 wt.% in the present study. To evaluate the effect of Zn content on the solidification behavior of the Mg–3RE alloy, the Pseudo–ternary Mg–RE–Zn phase diagrams (0.5 and 1.0 Zn addition) were calculated and presented in Fig. 2(c) and (d). One can see that with the addition of 0.5 and 1.0 Zn, solidification of the Mg–3RE alloy starts with the formation of primary α-Mg, followed by the formation of $Mg_{12}RE$ phase, and ends with the formation of α-Mg+$Mg_{12}RE$+MgZn eutectic. Besides, with increasing Zn content from 0 to 1, the liquidus temperature keeps almost invariable while the solidification ranges of the Mg–3RE alloy increase. It has been reported that the increased solidification ranges because of increasing Zn content could result in the increase of hot-tearing susceptibility during HPDC [23]. Moreover, the effect of Zn on the maximum solid solubility of Mg–RE alloys and precipitation temperatures of Zn-containing phases were investigated.

As shown in Fig.2(d), the maximum solid solubility of RE in α–Mg is decreased from 1.2 to 0.9 wt.% with increasing Zn from 0.0 to 1.0 wt.%, indicating that Zn can promote the precipitation of the $Mg_{12}RE$ phase, which benefit to improving the thermal conductivity due to the decrease of solute atoms in the α-Mg matrix. The precipitation temperature (PT) of the MgZn phase increases from 55 to 98 °C with increasing Zn content from 0.5 to 1.0 wt.%. For avoiding the hot tearing and formation of the MgZn phase, the 0.5 wt.% Zn was added and the casting mold was preheated to ~260 °C. Based on the above thermo-calc calculation and analysis, the alloying compositions were designed as Mg–3.0RE–0.5Zn.

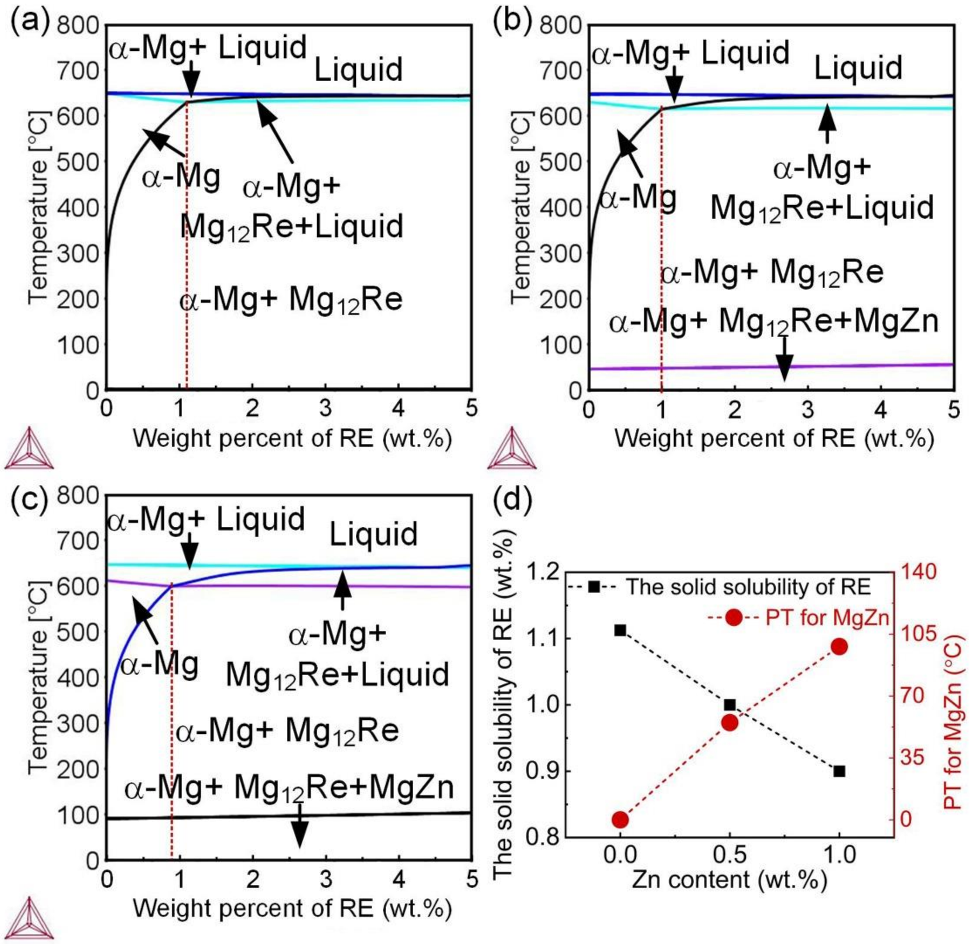


Fig. 2. Isopleths along RE axis through Mg–RE(Ce and La)–Zn pseudo-ternary phase diagram at various Zn additions with a RE content of 0–5 wt.%: (a) 0.0 wt.% Zn, (b) 0.5 wt.% Zn, and (c) 1.0 wt.% Zn; (d) the maximum solid solubility of RE in α-Mg and precipitation temperature (PT) of MgZn as function of Zn contents.

Table 1 lists the room-temperature thermal properties and density of the HPDC EZ30 alloy. The thermal conductivity of the biscuit (location 1) and casting body (location 2) is calculated from the thermal diffusivity, specific heat capacity, and density. It can be seen that there is a small difference in both heat capacity and density between the biscuit and casting body, while the casting body shows lower thermal diffusivity than that of the biscuit. The thermal conductivity of the biscuit and casting body is measured to be 144.7 $W(m\cdot K)^{-1}$ and 133.9 $W(m\cdot K)^{-1}$, respectively, indicating a decrease in the thermal conductivity of the casting body compared to the biscuit. The thermal conductivity of the casting body determines the level of heat dissipation for cellphone components.

Table 1 Thermal properties and density of the studied alloy at room temperature

| Samples | thermal diffusivity $\alpha$ / $mm^2 \cdot s^{-1}$ | special heat capacity $C_p$ /J $(g \cdot K)^{-1}$ | Density $\rho$ / $g \cdot cm^{-3}$ | thermal conductivity $\kappa$ / $W(m \cdot K)^{-1}$ |
|---|---|---|---|---|
| Biscuit | 80.528 | 1.008 | 1.783 | 144.7 |
| Casting body | 74.167 | 1.010 | 1.785 | 133.9 |

Fig. 3(a) presents the representative engineering stress-strain curves of the casting body, and the average tensile properties are summarized in Table 2. One can see that the alloy exhibits excellent room-temperature mechanical properties with 0.2% yield strength of ~153 MPa, ultimate tensile strength of ~195 MPa, and elongation of ~4.3%. For comparison, the thermal conductivity and yield strength of some as-cast Mg alloys in published literatures are displayed in Fig. 3(b). It can be seen that the HPDC EZ30 alloy exhibits both high thermal conductivity and high YS than the Mg–Al series, Mg–Mn series, Mg–RE series, and most Mg–Zn series, indicating an excellent combination of high thermal conductivity and high strength. The reason is disclosed based on its phase constitution and microstructure characteristics.

Table 2 Tensile properties of the casting body at room temperature

| Alloy | Yield Strength $\sigma_{0.2}$ / MPa | Ultimate Tensile Strength $\sigma_b$ / MPa | Elongation $\varepsilon$ / % |
|---|---|---|---|
| EZ30 | $153^{+2}_{-3}$ | $195^{+2}_{-4}$ | $4.3^{+0.2}_{-0.2}$ |

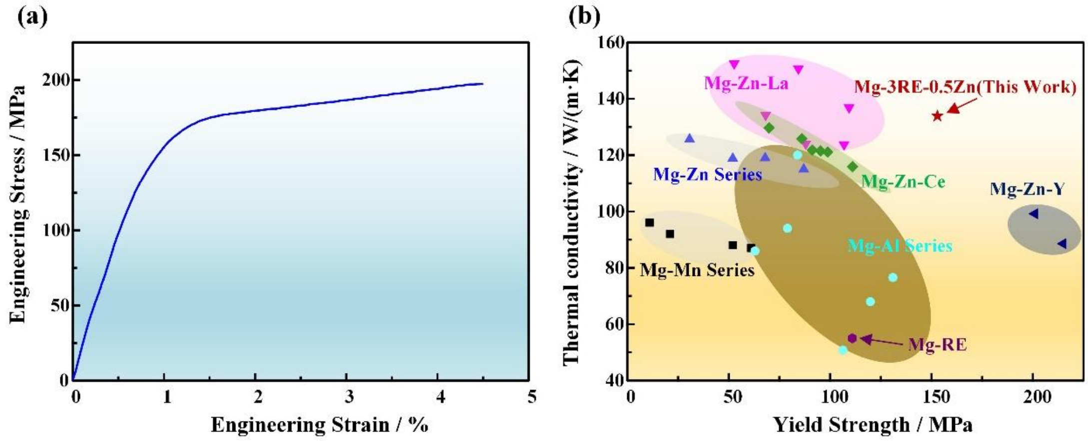


Fig. 3. (a) tensile engineering stress-strain curves of the casting body at room temperature; (b) thermal conductivity and yield strength of some Mg alloys in casting condition [9, 10, 22, 23]

XRD pattern reveals that the casting body is composed of α-Mg and $Mg_{12}RE$ phases (Fig. 4(a)), which is similar to previous results [24, 25]. MgZn phase cannot be detected in the alloy, which can be attributed to the combination of low content Zn addition and high mold temperature (~260°C). It has been reported that the $Mg_{12}RE$ eutectic phase can easily form during the solidification of the Mg–Ce/La system alloys because of its relatively low barrier to nucleation and relative thermodynamic stability [26, 27]. Moreover, Zn addition into Mg–RE alloys can increase the nucleation sites and promote the formation for $Mg_{12}RE$ phase (Fig. 2(d)) [22]. The DTA cooling curve shown in Fig. 4(b) are used to speculate the phase formation during solidification, where each exothermic peak denotes the formation of the phase labeled. The exothermic peaks corresponding to the formation of α-Mg and $Mg_{12}RE$ are approximately 633 °C and 586 °C, respectively. According to the results of thermos-calc calculation, XRD analysis, and DTA curve, thus, the solidification behavior of the alloy is basically as following: L→α-Mg + L →α-Mg + $Mg_{12}RE$ + L→α-Mg + $Mg_{12}RE$.

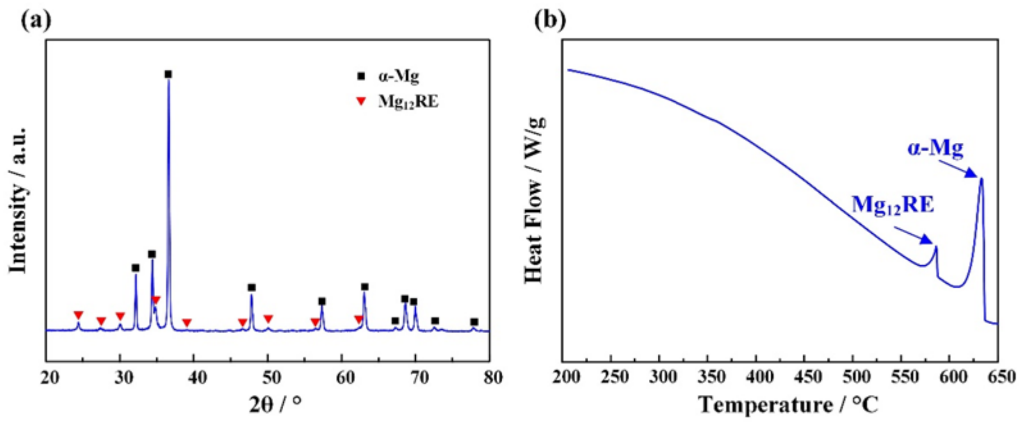


Fig. 4. (a) X-ray diffraction pattern and (b) DTA cooling curve of the casting body

Fig. 5(a) and (b) show optical images of HPDC EZ30 alloy taken from the casting body. One can see from Fig. 5(a) that a small number of porosities (marked by white arrows) with sizes ranging from 5 μm to 30 μm can be observed in the alloy, indicating good compactness. As shown in Fig. 5(b), the HPDC EZ30 alloy exhibits a fine homogeneous equiaxed grain structure with an average grain size of ~4.3 μm, which is comparable with the traditional HPDC Mg–RE based alloys with an average grain size of 5−20 μm. To further investigated the morphology and distribution of the $Mg_{12}RE$ phase, typical back-scattered SEM images are presented in Fig. 5(c) and (d). It can be seen that numerous networked eutectic phases with bright contrast are concentrated at grain boundaries, as marked by the yellow arrows. According to the calculation and experimental results in the HPDC

Mg-4Ce-0.5Mn alloy, Su et al. [28] confirmed that the primary Mg solution phase was generated first from the liquid and pushed alloying elements into the interdendritic regions, where the binary eutectic reactions occur at high temperature. Therefore, primary Mg phases were surrounded by networked $Mg_{12}Ce$ eutectic phases. For the HPDC EZ30 alloy, the growth of primary α–Mg crystals is restrained by networked eutectic phases concentrated at grain boundaries and the fast cooling rate during the solidification, which is responsible for the fine grains (~4.3 μm).

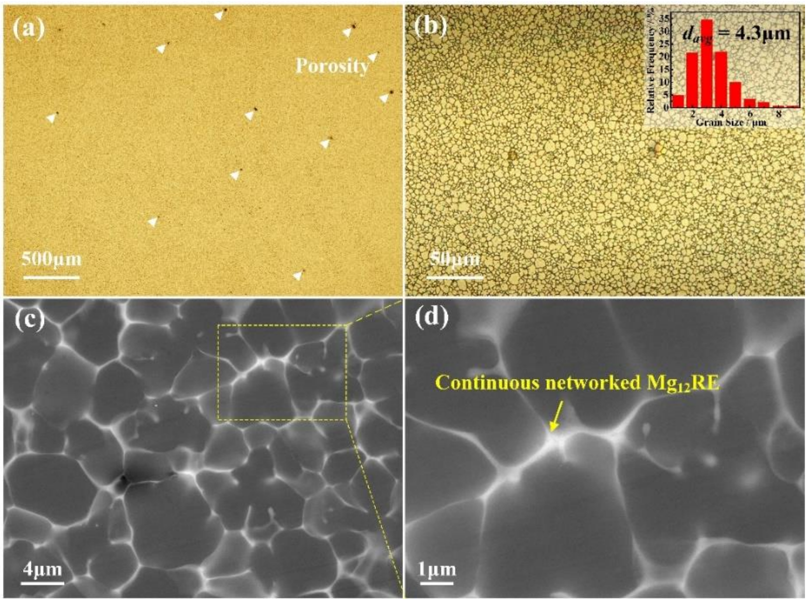


Fig. 5. (a) and (b) optical images of the casting body; (c) and (d) typical back-scattered SEM images of the casting body; inset: $d_{avg}$ stands for the average grain size

Fig. 6 (a)–(d) shows the typical bright-field TEM images and corresponding selected area electron diffraction (SAED) patterns taken from the casting body of HPDC EZ30 alloy. As seen from Fig. 6(a) and (b), the networked divorced eutectic phases are consistent with SEM observations and similar with the networked $Mg_{12}RE$ eutectic phase reported in the Mg–Ce/La alloys [17, 25]. The SAED patterns (shown in Fig. 6(c) and (d)) taken from the eutectic phase confirm that the networked phase is $Mg_{12}Ce$ isomorphous phase with body-centered tetragonal structure and space group of *I4/mmm*. The measured lattice parameters of this phase are $a$ = 1.0322 nm and $c$ = 0.594 nm. EDS analysis (Fig. 6(e)) illustrates its chemical composition is 89.22Mg, 2.93Zn, 4.72Ce, and 3.13La (at.%), where the atomic ratio of (Mg+Zn)/(Ce+La) is 11.7, close to 12, suggesting that the networked intermetallic is $(Mg, Zn)_{12}RE$ with Zn atoms partly occupying the Mg sites. A similar result has been reported in the HPDC Mg–4Zn–2La–3Y alloy, where the Zn segregates in the

$Mg_{12}RE$ intermetallic phase [22]. Moreover, the EDS spectrum in Fig. 6(f) indicates that the α-Mg matrix contains rare solute atoms. Therefore, it can be concluded that the REs and Zn elements in the HPDC EZ30 alloy mainly exist in the form of the networked $(Mg, Zn)_{12}RE$ eutectic phase.

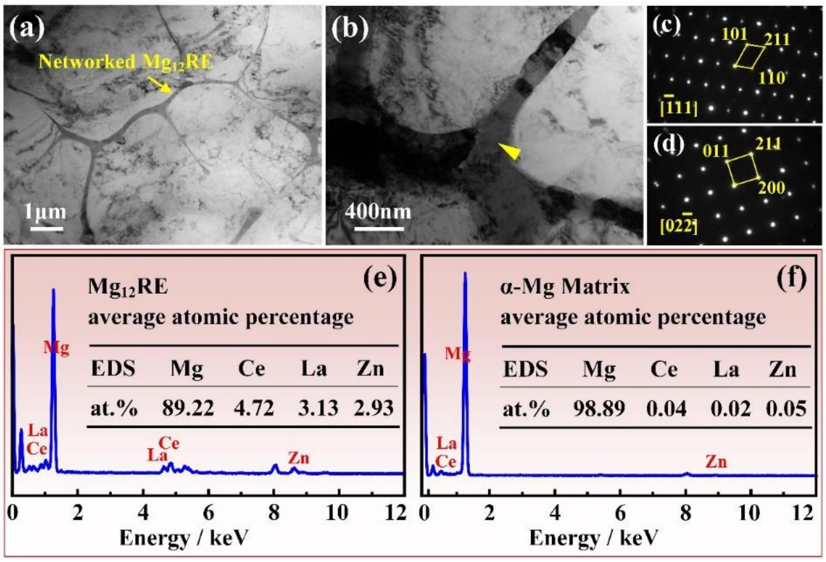


Fig. 6. (a) and (b) bright-field TEM images of the casting body; (c) and (d) corresponding SAED patterns taken from the networked intermetallic indicated by the yellow arrow in (b); (e) and (f) EDS spectrums of the networked intermetallic and α-Mg matrix, respectively.

For comparison, the phase constituent and microstructure characterization of the biscuit are also investigated and presented in Fig. 7. As shown in Fig. 7(a), the XRD analysis result of the biscuit is consistent with that of the casting body (Fig. 4(a)), where only the $Mg_{12}RE$ phase can be detected in addition to the α-Mg matrix phase. Furthermore, there is an obvious difference in microstructure between the biscuit and casting body. Compared to the fine homogeneous grain structure of the casting body, coarser and inhomogeneous grain structure can be observed in the microstructure of the biscuit (Fig. 7(b)). And the microstructure of the biscuit also consists of continuous networked eutectic phases distributed along grain boundaries. Corresponding EDS element mappings (Fig. 7(d)-(g)) indicate that the networked eutectic phases are enriched with Ce, La, and Zn elements. EDS analysis (Fig. 7(h)) shows the average chemical composition of the networked eutectic phase and reveals that the atomic ratio of (Mg, Zn)/(La, Ce) is 11.5, which is close to 12 for $Mg_{12}RE$ phases. According to the XRD analysis and EDS results, it can be confirmed that the networked eutectic phase of the biscuit is $(Mg, Zn)_{12}RE$, which is the same as that of the casting body. Moreover, the total concentrations of solute atoms in the α-Mg matrix of the biscuit are significantly low (0.08 at.%), which is similar to that of the casting body. The reason is that the formation of (Mg, Zn)$_{12}$RE eutectic phase almost completely consumed the REs and Zn elements.

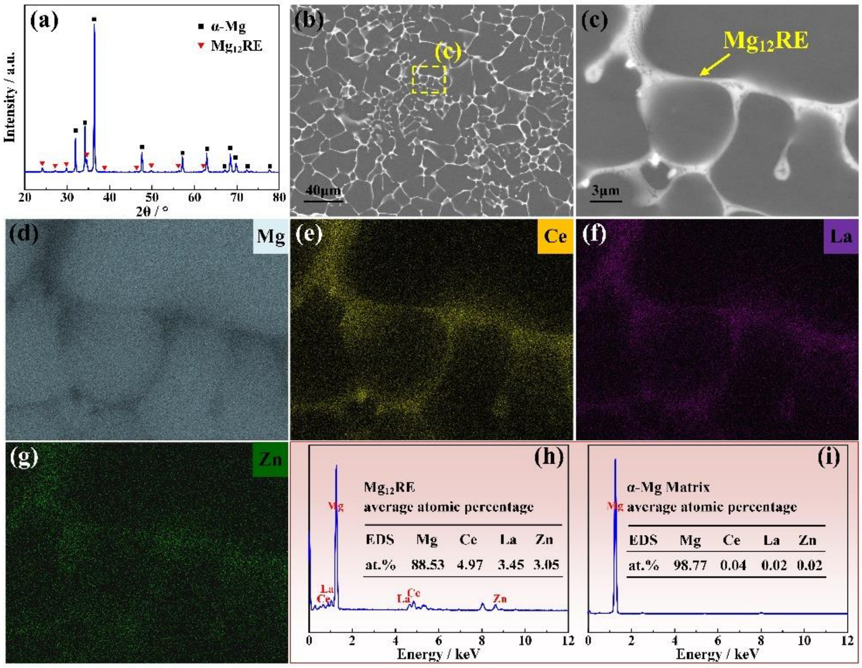


Fig. 7. (a) X-ray diffraction pattern and (b), (c) back-scattered SEM micrographs of the biscuit; (d)-(g) corresponding element mapping of Mg, Ce, La, and Zn, respectively; (h) and (i) EDS spectrums of the networked eutectic phase and α-Mg matrix, respectively.

The thermal conductivity of Mg alloys is generally influenced by solution atoms and second phases, which will induce the lattice distortion and thus scatter free electron and phonon movement, resulting in the reduction in thermal conductivity [9, 15, 29]. The adverse effect on thermal conductivity caused by the solute atoms is known to be approximately several orders larger than that by the second phase [15, 16]. Li et al. investigated the effect of RE elements present in solid solution and intermetallic on the thermal conductivities of Mg–RE alloys, and revealed that the reduction in thermal conductivity was approximately 123.0 W/(m·K) with per 1 at.% RE addition in the form of solute atoms or 6.5–16.4 W/(m·K) in the form of Mg–RE intermetallic [15]. Moreover, Xie et al. studied the influence of RE-containing intermetallic on the thermal conductivity of Mg–La/Ce–Zn alloys, and the results indicated that the Mg$_{12}$RE intermetallic showed a slight impact on decreasing the thermal conductivities [25].

The microstructural observations have further confirmed that the alloying elements (REs and Zn) in both biscuit and casting body are largely consumed by the formation of the networked (Mg, Zn)$_{12}$RE eutectic phases (Figs. 6 and 7), resulting in significantly low concentrations of alloying elements dissolved in the α–Mg matrix. Thus, the lattice distortion produced by solute atoms and networked (Mg, Zn)$_{12}$RE eutectic phases seems to be weak, which accounts for the high thermal conductivity (144.7 W/(m·K) of the biscuit and 133.9 W/(m·K) of the casting body. Compared to the biscuit, the decrease in thermal conductivity of the casting body is mainly ascribed to the much finer grain size, which means higher volume fractions of grain boundaries. The increased volume fractions of grain boundaries in the casting body can act as the scattering sources blocking the free movement of electrons and thus decreasing thermal conductivity [7]. It has been reported that the contents of Al solute atoms in the thin-walled AZ91D specimen (~6.23 at.%) were much higher than that in the traditional HPDC AZ91D specimens (~3.67 at.%) due to the rapid cooling rate [7, 30]. The actual thermal conductivity of the thin-walled AZ91D specimen was lower than that of the traditional HPDC AZ91D specimens due to more serious lattice distortion induced by more solute atoms. Therefore, it can be concluded that Mg-Al based alloys containing high Al contents are not suitable as the thin-walled products with high thermal conductivity. For comparison, the EZ30 alloy shows great potential as thin-walled components with high thermal conductivity, owing to the addition of alloying elements with low solubility and the alloying elements largely consumed by the formation of (Mg, Zn)$_{12}$RE eutectic phases.

It is well known that fine-grain strengthening, second phase strengthening, and solid solution strengthening are the main strengthening mechanisms of Mg alloys [31, 32]. Moreover, Gavras et al. reported that the YS of the HPDC Mg-RE alloys was attributed to the contribution from key strengthening factors, including fine-grain strengthening that is related to the Hall–Petch relationship ($\sigma_{gb}$), solid solution strengthening ($\sigma_{ss}$), and grain boundary reinforcement present at grain and cell boundaries from the RE-containing intermetallic ($\sigma_{Mg\text{–}RE}$) [33, 34]. Thus, in this study, the YS of the HPDC EZ30 alloy can be estimated by the following equation:

$$\sigma_{Mg\text{-}3RE\text{-}0.5Zn} = \sigma_{gb} + \sigma_{ss} + \sigma_{Mg\text{–}RE}$$

According to the Hall-Petch equation [35, 36], the YS contributed from grain boundary strengthening ($\sigma_{gb}$) is estimated to be ~125 MPa in this alloy with an average grain size of ~4.3 μm. Nevertheless, for Mg-Ce/La system alloy, solid solution strengthening from RE atoms is not the key strengthening component due to Ce and La with low solubility in the Mg matrix. For instance, Zhu et al. reported a die-cast Mg-2.5RE-0.6Zn alloy (wt.%, RE: rich in La) with a high YS of 136.3 (±5.4) MPa, owing to the fine grain structure with an average grain size of approximately 7 μm and high volume fraction of $Mg_{12}RE$ intermetallic phase distributed at grain boundaries [37]. In the present study, the solid solution strengthening ($\sigma_{ss}$) can be determined based on the following equation [22, 38]:

$$\Delta\sigma_{ss} = \alpha M G \varepsilon_{ss}^{2/3} C^{1/2}$$

where α represents a constant (1/550 in Mg), M represents the Taylor factor (3.06), G is the shear modulus of the Mg matrix (about 16.6 GPa), C is the concentration of the solute atoms, and $\varepsilon_{ss}$ is the misfit strain. According to the ESD result (Fig. 6(f)), the strength increment ($\sigma_{ss}$) from RE and Zn solutes is finally calculated to be ~6 MPa for the HPDC EZ30 alloy, revealing the weak strengthening effect due to the low content of solute atoms in the α-Mg matrix. Hence, the grain boundary reinforcement ($\sigma_{Mg\text{–}RE}$), contributed from networked $(Mg, Zn)_{12}RE$ intermetallic phase concentrated at grain boundaries, benefit to the YS is ~22 MPa. Chia et al. demonstrated that the YS of the binary HPDC Mg–La/Ce alloys was depended on the volume fraction of $Mg_{12}RE$ intermetallic and indicated that the HPDC Mg–2.87Ce (wt.%) and Mg–3.44La (wt.%) alloys showed a high YS of ~135 (±2) MPa and ~141 (±5) MPa, respectively [39]. The composition of the HPDC EZ30 alloy newly developed in this study is relatively similar to the Mg–2.87Ce and Mg–3.44La alloys, as is the volume fraction of the intermetallic phase. Compared with these two alloys, the studied alloy has finer and more homogeneous grain structures and thus exhibits higher strength. Additionally, Zn addition in the studied alloy can reinforce the strengthening effect by segregating in the $Mg_{12}RE$ intermetallic phase. Therefore, the high YS of the HPDC EZ30 alloy is mainly attributed to the combined strengthening effects of fine grain size (~4.3μm) and $(Mg, Zn)_{12}RE$ intermetallic phase (14.7%).

The tensile fracture morphology of the HPDC EZ30 alloy is presented in Fig. 8. As shown in Fig. 8(a), some porosities marked by the yellow arrows are observed in the fracture surface, which harms the ductility. It should be noted that the formation of porosities is inevitable in the HPDC alloys and can be controlled by optimizing the die-casting technique. Furthermore, it can be seen from Fig. 8(b) that the fractograph of EZ30 alloy exhibits typical intergranular fracture characteristics containing numerous clear ridges and smooth dissociation facets, which is consistent with the low elongation (4.3%) of the alloy. The reason is that the inevitable porosities and high volume fraction of coarse continuous networked $Mg_{12}RE$ intermetallic phases can easily cause stress concentration and acts as the source of micro-cracks, which results in low ductility.

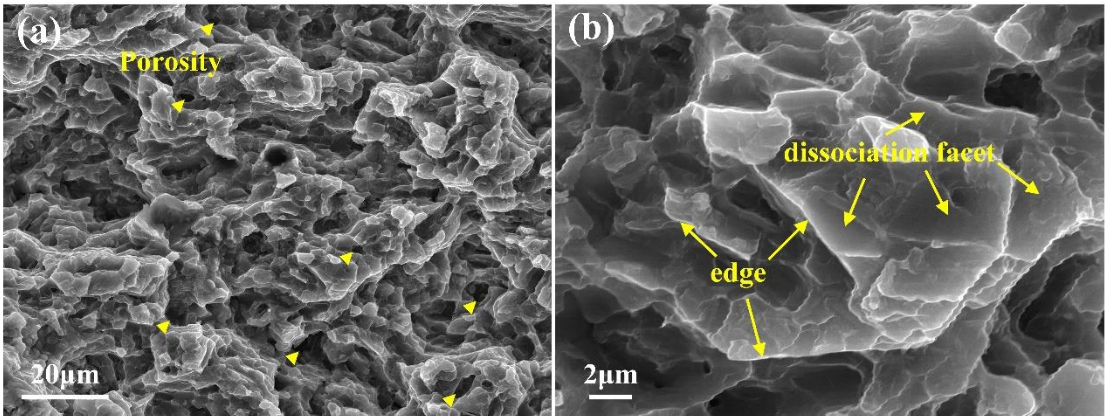


Fig. 8 SEM images of the tensile fracture for the casting body.

## 4. Conclusions

In summary, the HPDC Mg-3RE-0.5Zn alloy with superior thermal conductivity and high strength was developed. This alloy is suitable for the production of ultrathin wall cellphone components. The HPDC components exhibited high thermal conductivity of 133.9 W/(m·K) and good mechanical properties with YS of ~153 MPa, UTS of ~195 MPa, and elongation of ~4.3%. The high thermal conductivity was mainly attributed to the low content of solute atoms in the α-Mg matrix, and the high strength was responsible for fine grain structure and networked $(Mg, Zn)_{12}RE$ eutectic phase.

## Acknowledgments

The authors are grateful to the financial support by National Key Research and Development Program of China (No. 2016YFB0301103) and National Natural Science Foundation of China (NSFC, No. 51401010).

## References

[1] F. Wang, T. Hu, Y.T. Zhang, W.L. Xiao, C.L. Ma, Effects of Al and Zn contents on the microstructure and mechanical properties of Mg–Al–Zn–Ca magnesium alloys, Mater. Sci. Eng. A. 704 (2017) 57–65.

[2] H.C. Pan, F.S. Pan, R.M. Yang, J. Peng, C.Y. Zhao, J. She, Z.Y. Gao, A.T. Tang, Thermal and electrical conductivity of binary magnesium alloys, J. Mater. Sci. 49 (2014) 3107–3124.

[3] A. Rudajevova, F.V. Buch, B.L. Mordike, Thermal diffusivity and thermal conductivity of Mg–Sc alloys, J. Alloy Compd. 292 (1999) 27–33.

[4] X. Du, W.B. Du, Z.H. Wang, K. Liu, S.B. Li, Simultaneously improved mechanical and thermal properties of Mg-Zn-Zr alloy reinforced by ultra-low content of graphene nanoplatelets, Appl. Surf. Sci. 536 (2021) 147791.

[5] W.L. Xiao, M.A. Easton, S.M. Zhu, M.S. Dargusch, M.A. Gibson, S.S. Jia, J.F. Nie, Casting Defects and Mechanical Properties of High Pressure Die Cast Mg-Zn-Al-RE Alloys, Adv. Eng. Mater. 14 (2012) 68–76.

[6] W.J. Joost, P.E. Krajewski, Towards magnesium alloys for high-volume automotive applications, Scr. Mater. 128 (2017) 107–112.

[7] G.Y. Yuan, G.Q. You, S.L. Bai, W. Guo, Effects of heat treatment on the thermal properties of AZ91D magnesium alloys in different casting processes, J. Alloy. Compd. 766 (2018) 410–416.

[8] A. Rudajevová, P. Lukáˇ c, Comparison of the thermal properties of AM20 and AS21 magnesium alloys, Mater. Sci. Eng. A. 397 (2005) 16–21.

[9] S.B. Li, X.Y. Yang, J.T. Hou, W.B. Du, A review on thermal conductivity of magnesium and its alloys, J. Magnes. Alloy. 8 (2020) 78–90.

[10] Y.F. Liu, X.G. Qiao, Z.T. Li, Z.H. Xia, M.Y. Zheng, Effect of nano-precipitation on thermal conductivity and mechanical properties of Mg-2Mn-xLa alloys during hot extrusion, J. Alloy. Compd. 830 (2020) 154570.

[11] V.E. Bazhenov, A.V. Koltygin, M.C. Sung, S.H. Park, Yu.V. Tselovalnik, A.A. Stepashkin, A.A. Rizhsky, M.V. Belov, V.D. Belov, K.V. Malyutin, Development of Mg–Zn–Y–Zr casting magnesium alloy with high thermal conductivity, J. Magnes. Alloy. In Press.

[12] ASM Handbook, Properties and Selection: Nonferrous Alloys and Special-purpose Materials, 2, tenth ed., ASM International, Materials Park, 2002.

[13] B. Li, L. Hou, R. Wu, J. Zhang, X. Li, M. Zhang, A. Dong, B. Sun, Microstructure and thermal conductivity of Mg-2Zn-Zr alloy, J. Alloys Compd. 722 (2017) 772–777.

[14] J.W. Yuan, K. Zhang, X.H Zhang, X.G. Li, T. Li, Y.J. Li, M.L. Ma, G.L. Shi, Thermal characteristics of Mg–Zn–Mn alloys with high specific strength and high thermal conductivity, J. Alloy Compd. 578 (2013) 32–36.

[15] C.Y. Su, D.J. Li, A.A. Luo, T. Ying, X.Q. Zeng, Effect of solute atoms and second phases on the thermal conductivity of Mg-RE alloys: a quantitative study, J. Alloys Compd. 747 (2018) 431-437.

[16] C. Su, D. Li, T. Ying, L. Zhou, L. Li, X. Zeng, Effect of Nd content and heat treatment on the thermal conductivity of MgNd alloys, J. Alloy. Compd. 685 (2016) 114–121.

[17] S.M. Zhu, M.A. Gibson, M.A. Easton, J.F. Nie, The relationship between microstructure and creep resistance in die-cast magnesium–rare earth alloys, Scr. Mater. 63 (2010) 698–703.

[18] M. Celikin, A.A. Kaya, R. Gauvin, M. Pekguleryua, Effects of manganese on the microstructure and dynamic precipitation in creep-resistant cast Mg–Ce–Mn alloys, Scr. Mater. 66 (2012) 737–740.

[19] L.L. Rokhlin, Magnesium Alloys Containing Rare Earth Metals: Structure and Properties, Crc. Press, London, 2003.

[20] L.P. Zhong, J. Peng, M. Li, F.S. Pan, Effect of Ce addition on the microstructure, thermal conductivity and mechanical properties of Mg-0.5Mn alloys, J. Alloys Compd. 661 (2016) 402–410.

[21] S.M. Zhu, M.A. Easton, T.B. Abbott, J.F. Nie, M.S. Dargusch, N. Hort, M.A. Gibson,

Evaluation of Magnesium Die-Casting Alloys for Elevated Temperature Applications: Microstructure, Tensile Properties, and Creep Resistance, Metall. Mater. Trans. A. 46 (2015) 3543–3554.
[22] X.R. Hua, Q. Yang, D.D. Zhang, F.Z. Meng, C. Chen, Z.H. You, J.H. Zhang, S.H. Lv, J. Meng, Microstructures and mechanical properties of a newly developed high-pressure die casting Mg-Zn-RE alloy, J. Mater. Sci.Tech. 53 (2020) 174–184.
[23] V.E. Bazhenov, A.V. Koltygin, M.C. Sung, S.H. Park, A.Yu. Titov, V.A. Bautin, S.V. Matveev, M.V. Belov, V.D. Belov, K.V. Malyutin, Design of Mg–Zn–Si–Ca casting magnesium alloy with high thermal conductivity, J. Magnes. Alloy. 8 (2020) 184–191.
[24] Y.F. Liu, X.J. Jia, X.G. Qiao, S.W. Xu, M.Y. Zheng, Effect of La content on microstructure, thermal conductivity and mechanical properties of Mg–4Al magnesium alloys, J. Alloy. Compd. 806 (2019) 71–78.
[25] T.C. Xie, H. Shi, H.B. Wang, Q. Luo, Q. Li, Kuo-Chih Chou, Thermodynamic prediction of thermal diffusivity and thermal conductivity in Mg–Zn–La/Ce system, J. Mater. Sci.Tech. 97 (2022) 147–155.
[26] J. Grobner, A. Kozlov, R. Schmid-Fetzer, M.A. Easton, S. Zhu, M.A. Gibson, J.F. Nie, Thermodynamic analysis of as-cast and heat-treated microstructures of Mg–Ce–Nd alloy, Acta Mater., 59 (2011) 613–622.
[27] M.A. Easton, M.A. Gibson, D. Qiu, S.M. Zhu, J. Grobner, R. Schmid-Fetzer, J.F. Nie, M.X. Zhang, The role of crystallography and thermodynamics on phase selection in binary magnesium–rare earth (Ce or Nd) alloy, Acta Mater., 60 (2012) 4420–4430.
[28] C.Y. Su, D.J. Li, J. Wang, R.H. Shi, A.A. Luo, X.Q. Zeng, Z.H. Lin, J. Chen, Enhanced ductility in high-pressure die casting Mg-4Ce-xAl-0.5Mn alloys via modifying second phase, Mater. Sci. Eng. A. 773 (2020) 138870.
[29] Y.F. Liu, X.J. Jia, X.G. Qiao, S.W. Xu, M.Y. Zheng, Effect of La content on microstructure, thermal conductivity and mechanical properties of Mg–4Al magnesium alloys, J. Alloy. Compd. 806 (2019) 71–78.
[30] J. Rong, W.L. Xiao, X.Q. Zhao, C.L Ma, H.M. Liao, D.L. He, M. Chen, M. Huang, C. Huang, A high thermal conductivity and high strength magnesium alloy for high pressure die cast ultrathin-walled component. Int. J. Min. Met. Mater. Accepted.
[31] W.L. Xiao, M.A. Easton, M.S. Dargusch, S.M. Zhu, M.A. Gibson, The influence of Zn additions on the microstructure and creep resistance of high pressure die cast magnesium alloy AE44, Mater. Sci. Eng. A. 539 (2012) 177–184.
[32] H.Y. Wang, J. Rong, G.J. Liu, M. Zha, C. Wang, D. Luo, Q.C. Jiang, Effects of Zn on the microstructure and tensile properties of as-extruded Mg-8Al-2Sn alloy, Mater. Sci. Eng. A. 698 (2017) 249–255.
[33] S. Gavrasa, M.A. Eastona, M.A. Gibson, S.M. Zhu, J.F. Nie, Microstructure and property evaluation of high-pressure die-cast Mg–La–rare earth (Nd, Y or Gd) alloys, J. Alloy. Compd. 597 (2014) 21–29.
[34] H. C´aceresa, W.J. Poole, A.L. Bowles, C.J. Davidson, Section thickness, macrohardness and yield strength in high-pressure die cast magnesium alloy AZ91C, Mater. Sci. Eng. A. 402 (2005) 269–277.
[35] R.X. Zheng, J.P. Du, S. Gao, H. Somekawa, S. Ogata, N. Tsuji, Transition of dominant deformation mode in bulk polycrystalline pure Mg by ultra-grain refinement down to sub-

micrometer, Acta. Mater. 198 (2020) 35–46.
[36] J. Rong, P.Y. Wang, M. Zha, C. Wang, X.Y. Xu, H.Y. Wang, Q.C. Jiang, Development of a novel strength ductile Mg-7Al-5Zn alloy with high superplasticity processed by hard-plate rolling (HPR), J. Alloy. Compd. 738 (2018) 246–254.
[37] S.M. Zhu, M.A. Gibson, J.F. Nie, M.A. Easton, and G.L. Dunlop. (2009). Primary creep of die-cast magnesium–rare earth based alloys. Metall Mater Trans A. 40A(2009) 2036–2041.
[38] R.L. Fleischer, Substitutional solution hardening Durcissement de solution par substitution Verfestigung in substitutionsmischkkistallen. Acta Metall. 11 (1963) 203–209
[39] T.L. Chia, M.A. Easton, S.M. Zhu, M.A. Gibson, N. Birbilis, J.F. Nie, The effect of alloy composition on the microstructure and tensile properties of binary Mg-rare earth alloys. Intermetallics. 17 (2009) 481–490.